Dentomaxillofacial Radiology (2013) 42, 20120321

http://dmfr.birjournals.org

RESEARCH

Ultrashort echo time (UTE) MRI for the assessment of caries lesions

A-K Bracher[1], C Hofmann[1,2], A Bornstedt[1], E Hell[3], F Janke[2], J Ulrici[3], B Haller[2], M-A Geibel[4] and V Rasche*[,1]

[1]*Department of Internal Medicine II, University Hospital of Ulm, Ulm, Germany;* [2]*Department of Operative Dentistry and Periodontology, University Hospital of Ulm, Ulm, Germany;* [3]*Sirona Dental Systems GmbH, Bensheim, Germany;* [4]*Department of Oral and Maxillofacial Surgery, University Hospital of Ulm, Ulm, Germany*

Objective: Direct *in vivo* MRI of dental hard tissues by applying ultrashort echo time (UTE) MRI techniques has recently been reported. The objective of the presented study is to clinically evaluate the applicability of UTE MRI for the identification of caries lesions.
Methods: 40 randomly selected patients (mean age 41 ± 15 years) were enrolled in this study. 39 patients underwent a conventional clinical assessment, dental bitewing X-ray and a dental MRI investigation comprising a conventional turbo-spin echo (TSE) and a dedicated UTE scan. One patient had to be excluded owing to claustrophobia. In four patients, the clinical treatment of the lesions was documented by intraoral pictures, and the resulting volume of the cavity after excavation was documented by dental imprints and compared with the MRI findings.
Results: In total, 161 lesions were identified. 157 (97%) were visible in the UTE images, 27 (17%) in the conventional TSE images and 137 (85%) in the X-ray images. In total, 14 teeth could not be analysed by MR owing to artefacts caused by dental fillings. All lesions appear significantly larger in the UTE images as compared with the X-ray and TSE images. *In situ* measurements confirm the accuracy of the lesion dimensions as observed in the UTE images.
Conclusion: The presented data provide evidence that UTE MR imaging can be applied for the identification of caries lesions. Although the current data suggest an even higher sensitivity of UTE MRI, some limitations must be expected from dental fillings.
Dentomaxillofacial Radiology (2013) **42,** 20120321. doi: 10.1259/dmfr.20120321

Cite this article as: Bracher A-K, Hofmann C, Bornstedt A, Hell E, Janke F, Ulrici J, et al. Ultrashort echo time (UTE) MRI for the assessment of caries lesions. *Dentomaxillofac Radiol* 2013; **42:** 20120321.

Keywords: dental magnetic resonance imaging; ultrashort echo time; early detection of caries lesions

Introduction

MRI has proven excellent performance in assessing soft tissues and has become a mainstay imaging modality in medical diagnosis. However, its limited capability in assessing mineralized tissues and rising artefacts caused by dental fillings have so far restricted its wide application in dentistry.[1]

The potential of dental MRI was first discussed in 1981, but until now dental MRI has been applied only to typical radiological applications such as the identification of extracranial tumours, observation of the temporomandibular joint, implant planning, assessment of dental and periapical anatomy and pathology and for the localization of impacted teeth.[2–17]

The inability to visualize hard tissue structures has prevented conventional MRI techniques from depicting the highly mineralized components of the tooth like dentine (which comprises up to 70% mineral hydroxylapatite, about 20% organic material and only 10% water)

*Correspondence to: Professor Volker Rasche, Department of Internal Medicine II, University Hospital of Ulm, Albert-Einstein-Allee 23, 89081 Ulm, Germany. E-mail: volker.rasche@uni-ulm.de
Received 13 September 2012; revised 14 November 2012; accepted 16 November 2012

and enamel (with a mineral content of up to 96%). The high mineral content of these structures causes a low concentration of free protons, resulting in only weak magnetization and a random dephasing at the susceptibility interfaces, causing rapid T_2 relaxation below 1 ms for dentine and below 250 μs for enamel.[18,19]

Several *in vitro* studies on the visualization of mineral structures of the teeth were published using stray field imaging (STRAFI), single and multinuclear solid state techniques, single-point imaging (SPI) and ultra-short echo time techniques like sweep imaging with Fourier transformation (SWIFT), zero echo time imaging and Ultrashort Echo time (UTE) imaging. For acquisition time constraints, most of the techniques cannot directly be translated to *in vivo* applications. First results of an *in vivo* depiction of the mineral structures of the teeth were shown by Gatehouse et al[26] and Boujraf et al[27] by applying a modified UTE technique.[20–27]

The mineral structures (primarily enamel) pass through an alternate cycle of mineral loss and gain in the hydroxylapatite crystal. Dental caries represents a sugar-dependent infectious disease that damages the structures of teeth. Acid-producing bacteria lead to a destabilization of the constant state of back-and-forth demineralization and remineralization of the tooth and demineralization proceeds faster than remineralization, thus causing demineralization of the teeth and later on caries lesions. During the progression of lesion formation, initially a local increase in liquid content with only moderate breakdown of the mineral structures occurs. The increase is caused by the local production of acid by the related bacterial inflammation and by saliva penetrating into the lesion through the porous demineralized enamel layer. Advanced progression leads to an increasing decay of the mineral structures, finally causing a substantial breakdown with related cavity formation.[28]

From an MRI point of view, both processes likely cause an increase of the local MRI signal by (a) increasing the local proton concentration and (b) increasing T_2^* relaxation rates owing to the mineral decomposition, which causes a local reduction of the susceptibility interfaces.[29]

MRI for the detection of caries lesions has been shown for *in vitro* and *in vivo* applications using an indirect or direct visualization approach. For indirect visualization, the teeth were embedded in a dedicated signal-providing material, whereas in the direct approach, the mineralized structures of the teeth were assessed.[25,29,30–32]

Indirect imaging of caries lesions with conventional spin echo techniques was published by Tymofiyeva et al.[33] Contrast between the teeth and the surrounding tissue was achieved by adding a contrast agent in the oral cavity. The observed signal enhancement in regions of degeneration of the tooth was attributed to the penetration of the contrast medium into the demineralized tooth substance.

The application of UTE imaging to detect early mineralization and caries lesions was recently presented in a feasibility study.[29] In this study, 12 patients were enrolled for initial assessment of the potential of UTE for identification of caries lesions. In direct comparison with intraoral bitewing X-ray, the UTE technique showed a 100% sensitivity, whereas in the conventional turbo-spin echo (TSE) technique, only 19% of the lesions could be identified. Several lesions were solely identified by UTE MRI. These lesions were attributed to early caries processes causing a local increase of unbound water molecules but no or only very limited breakdown of the mineral structure. This conclusion was supported by T_2^* and dimension quantification of the different lesion types. Although indicating a clear potential for the identification of early demineralization and caries lesions, the clinical applicability of the technique could not be evaluated fully, since the enrolled patients had only a limited number of metal fillings and crowns, prone to cause severe image degradation in MRI. Furthermore, only a single lesion mainly visible by UTE could be further investigated clinically.

It is the objective of this study to validate the clinical applicability and to proof the sensitivity of the three-dimensional (3D) UTE MRI technique for early identification of demineralization and caries lesions in humans. For that purpose, 28 additional patients have been enrolled to form a patient cohort of 40 patients in total. In all patients, the proposed UTE technique is evaluated and compared with conventional spin echo MRI and intraoral bitewing X-ray; limitations rising from metal artefacts are assessed and the appearance of the lesions in 3D UTE is validated by imprints in three more patients.

Materials and methods

Patients

40 randomly selected patients (16 female, 24 male, mean age 41 ± 15 years) with suspected caries lesions were enrolled in this clinical study. The image protocol was approved by the local ethics committee (no. 08/19) and written informed consent was obtained from all patients prior to the dental MRI examination.

In total, the patients had gold ($n = 3$), cement ($n = 24$), amalgam ($n = 104$) and composite ($n = 267$) fillings and gold ($n = 70$) and ceramic ($n = 6$) crowns. Patients with brackets or retainers were excluded from this study owing to the expected artefacts in the MR images as a result of the high nickel and cobalt contents in the alloys.

Study protocol

Prior to the MR examination all patients underwent a clinical investigation, including optical assessment and an intraoral bitewing X-ray of the suspicious areas. All bitewing images were acquired according to a standardized protocol in parallel imaging technique as described by Whaites.[34]

The MR examination was accomplished within 14 days after the initial investigation, prior to any dental treatment of the lesions.

All MR imaging was performed on a clinical 3 Tesla whole-body MRI system (Achieva; Philips Healthcare, Best, Netherlands) and the data were acquired with a single element (65×50 mm) of a 2×2 channel prototype carotid coil (Philips Research Europe, Hamburg, Germany; Figure1a). The coil was placed at the respective side of the jaw and then affixed with a Vac-Lok neck cushion (CIVCO Medical Solutions, Kalona, IA). Sandbags were placed on the left and right side of the head to avoid patient motion during the examination.

Each patient underwent the same MR imaging protocol, including two orthogonal surveys, a coil-sensitivity reference scan and two diagnostic scans: a multislice turbo-spin echo (MS TSE) and a 3D ultrashort echo time (3D UTE) sequence for caries lesion assessment.

The surveys were planned along the jaw in parasagittal and transversal direction to assess the optimal position of the coil. If necessary, the coil was repositioned and the scan was repeated. The coil sensitivity reference scan was used later on to homogenize the signal intensity of the images acquired by the prototype surface coil.

Two-dimensional MS TSE acquisitions with an in-plane resolution of 0.4×0.4 mm and a slice thickness of 1 mm and a 3D UTE sequence with an isotropic resolution of 0.8 mm^3 were applied (for detailed acquisition parameters, please refer to Table 1). The MS TSE sequence was included in the imaging protocol for verification of the performance of the conventional MR techniques in detection of caries lesions and early demineralization. The MS TSE scan was planned in parasagittal direction along the jaw (Figure 1b). The central point of the spherical field of view of the 3D UTE sequence was placed between the molars and premolars in transversal direction (Figure 1c) and between the lower and the upper jaw in sagittal direction (Figure 1d).

After the MR examination all patients underwent standard clinical dental treatment. Four patients were randomly selected for *in situ* documentation. Intra- and extraoral pictures were taken prior to the treatment and after fissure sealant or filling removal, excavation and filling. The excavation was controlled by caries detector fluid (1% acid red) plus frequent manual exploration of the hardness of the dentine. For documentation of the lesion extend, a bitewing X-ray of the post-excavation impression was acquired, which was used for qualitative validation of the lesion size.

Data analysis

For analysis, all data were transferred to a medical workstation (ViewForum; Philips Healthcare). The

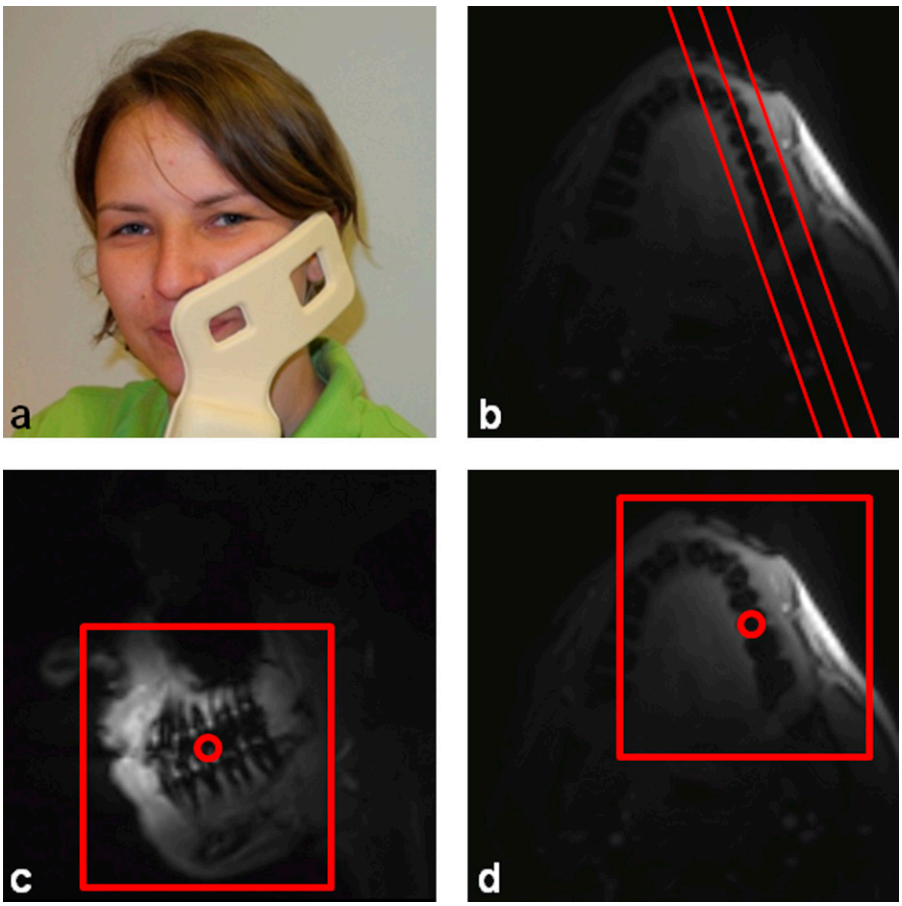

Figure 1 (a) Position of the prototype coil at one side of the jaw and planning of the (b) turbo-spin echo sequence along the jaw and the ultrashort echo time sequence in (c) parasagittal and (d) transverse direction

Table 1 MRI sequence parameter

Parameter	*HR-TSE*	*3D UTE*
Technique	Turbo-spin echo	Spoiled FID
Excitation	Slice selective	Non-slice selective
Flip angle (°)	90	10
RF pulse duration (ms)	4.2	0.05
Echo time (ms)	8.1	0.05
Repetition time (ms)	625	5
Number of echoes	16	1
Acquired resolution (mm^3)	$0.4 \times 0.4 \times 1$	$0.8 \times 0.8 \times 0.8$
Field of view (mm^3)	$230 \times 230 \times 8$	$120 \times 120 \times 120$
Scan time	5:32	7:49

3D UTE, three-dimensional ultrashort echo time; HR TSE, high spatial resolution turbo-spin echo; FID, free induction decay; RF, radiofrequency.

3D UTE scan was reconstructed at a resolution of $0.5 \times 0.5 \times 0.5\ mm^3$ and reformatted along the jaw in similar scan orientation as the MS TSE images.

Owing to the local demineralization and concomitant accumulation of acids and saliva in the caries lesion, the proton density and the local T_2/T_2^* are supposed to increase, causing a local signal enhancement.[29] Regions inside a tooth were defined as a caries lesion if they showed a signal brighter than the mean value plus two times the standard deviation of the surrounding tooth that did not belong to the pulp.

In all image modalities, height h, width w and the area A of identified lesions as well as the minimal distance between the lesion and the pulp d_{pulp} were measured. In the 3D UTE MR images, additional measurement of the lesion depth d was performed. Since a standardized parallel imaging technique was used for the intraoral bitewing X-rays, no correction for the projection geometry was performed.

For each identified lesion, the signal-to-noise ratio (SNR) and the contrast-to-noise ratio (CNR) were determined. For the estimation of the noise, the standard deviation of dentine of the affected tooth was used. Since the dentine shows very low signal, the related noise is very close to the background noise in air as used in conventional SNR/CNR measurements and only a little affected by the fast varying sensitivity pattern of the coil. The SNR was measured as the mean intensity and the respective standard deviation of the dentine. The CNR was determined by the difference between the mean intensity of the lesion and the dentine divided by the respective standard deviation of the dentine.

The lesion size in the X-ray image of the impression was qualitatively compared with the results of the *in vivo* MR and X-ray images.

All data were evaluated by an experienced dentist in consensus with an experienced MR scientist for providing expertise in the special contrast and artefact behaviour of the UTE sequence.

Statistical analyses

For statistical analysis, the lesions were divided into three different classes (CI, CII and CIII). Lesions of class CI are clearly visible in all three image types (X-ray, 3D UTE and MS TSE). CII lesions are clearly visible in the X-ray and 3D UTE images but not visible in the MS TSE images, and CIII lesions are solely visible in 3D UTE.

The lesion extensions in two dimensions (width and height) and the area of the lesion as well as the distance between the lesion and the pulp were compared between the X-ray, 3D UTE and MS TSE images.

To assess the statistical significance of the resulting differences between the investigated techniques, a two tailed paired t-test with a two-sample equal (homoscedastic) variance was used. Differences were considered significant for $p < 0.05$.

Results

The imaging protocol could be completed in 39 patients. One patient had to be excluded owing to claustrophobia. Including the repositioning of the coil between the left and the right jaw as well as the planning of the MR scans, the dental examination could be completed in less than 45 min. The measurement procedure and the scan times were well tolerated by the patients. Two patients had to be excluded owing to severe image degradation caused by 2 osteosynthesis plates, 12 gold crowns and 10 amalgam fillings. All other artefacts caused by dental filling materials were restricted to local distortions, which were limited to a single tooth ($n = 9$) or at maximum to adjacent teeth ($n = 2$). In total, 14 teeth could not be evaluated by either MRI approaches owing to the severe image degradation caused by dental filling materials.

Figure 2 exemplarily shows the appearance of a CII lesion in a molar in 3D UTE, reformatted in three orthogonal orientations, and the respective measurements of the lesion dimensions.

Owing to the strong decay of the coil sensitivity profile, the image quality was strongly depending on the distance between the coil and the teeth. All MR scans showed a distinguishable delineation between the pulp and the mineralized structures (dentine/enamel) of the teeth. A clear delineation between dentine and enamel layers could not be achieved in all patients. Especially in cases where the distance between the coil and the centre of the molars exceeded 2.5 cm, the resulting poor SNR limited the visibility of the dentine.

In total, 157 lesions were identified by 3D UTE, 137 lesions by X-ray, and 27 lesions were visible in the MS TSE images. In 4 out of the 14 teeth not accessible by MRI, a caries lesion was identified on the respective X-ray images. 24 lesions were solely identified by 3D UTE. These were either secondary lesions ($n = 6$), in which the dental filling material obstructed the lesion, occlusal lesions ($n = 3$), or very small, likely initial, caries lesions ($n = 15$). Assuming a total of 161 (157 identified by 3D UTE plus 4 additional lesions identified by X-ray only) caries lesions yielded a sensitivity of 97% for 3D UTE, 85% for X-ray and 17% for MS TSE.

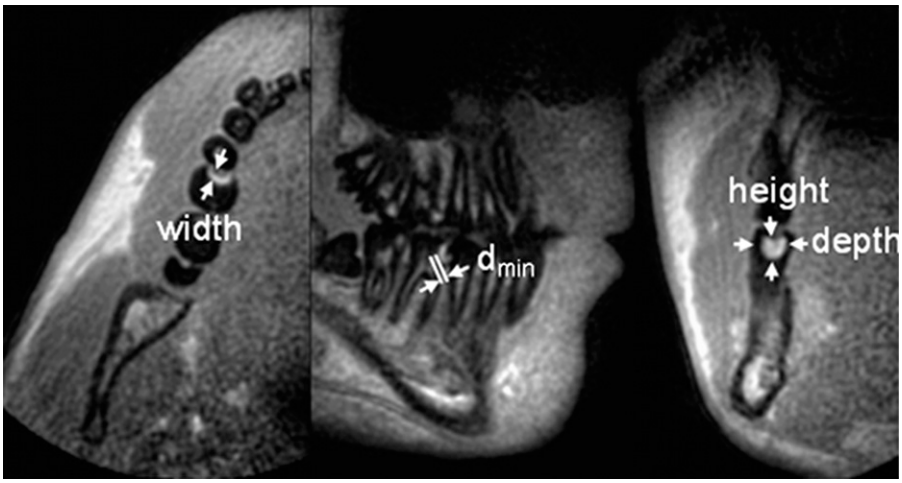

Figure 2 Transversal, parasagittal and coronal perspective of the teeth at the right side of the jaw

The lesions were categorized as CI lesions ($n = 25$), CII lesions ($n = 108$) and CIII lesions ($n = 24$), respectively.

Compared with the X-ray (CI and CII lesions) and MS TSE (CI lesions) images, all lesions appeared larger in the 3D UTE images. Lesions in MS TSE appeared much smaller than the X-ray findings. The distance between the lesion and the pulp varied because of the different lesion sizes between the three imaging approaches. Many lesions, which appeared in safe distance to the dental pulp in the X-ray image, almost reached its direct proximity in the 3D UTE images.

The *in vivo* SNR measurements resulted in a mean SNR value of 20 ± 10.6 for all lesions. For the CNR measurements, the mean value resulted in 16.2 ± 10.0. No significant differences between the lesion classes CI–CIII were observed for the SNR as well as for the CNR measurements.

The quantitative measurements and respective statistical significance for all three imaging approaches and lesion categories are summarised in Figures 3 and 4.

The extension of the CI lesions in the MS TSE images showed significant lower values ($p < 0.01$ for width, height and area) compared with the X-ray and 3D UTE findings. The results of the measurements in the 3D UTE images showed significantly higher values for the width ($p < 0.05$), height ($p < 0.01$) and area ($p < 0.01$) compared with the lesion extensions in the X-ray images. When compared with the other modalities, the minimal distance between the lesion and the pulp (d_{pulp}) showed significantly smaller values in the 3D UTE than the respective MS TSE ($p < 0.01$) and X-ray ($p < 0.01$) images but no significant differences between MS TSE and X-ray ($p = 0.22$) images.

For CII lesions, the differences of the lesion extensions between 3D UTE and X-ray images showed significant values for width, height, area and distance (d_{pulp}) ($p < 0.01$ for all geometrical properties).

For interclass comparison, the distance (d_{pulp}) and the lesion extension in all three directions (width, depth and height) as well as the area of all visible lesions in the 3D UTE images were compared (Figure 4). Differences between CI and CIII as well as between CII and CIII of the lesion size in all three directions were significant. CIII lesions showed smaller lesion extensions than with CI as well as with CII lesions. Comparing the lesion size of CI and CII lesions, only the lesion width showed no significant lower values for the CII lesions ($p = 0.1$). In the UTE images, the distance between the lesion and the pulp showed significant higher values for CIII lesions than with CI ($p < 0.01$) and CII ($p < 0.05$) lesions but showed only a trend to lower values for CI than for CII ($p = 0.09$) lesions.

The *in situ* documentation includes examples for each category (CI, CII and CIII). Respective intraoral pictures prior to and after dental treatment, MR and X-ray images are shown in Figures 5–7. All lesions are labelled with a white arrow in the MR images and a black arrow in the X-ray images.

Figure 5a shows an approximal CI (lesion 1) and lingual CI (lesion 2, Figure 5b) smooth surface caries. Both lesions are clearly visible in the intraoral pictures as well as in the X-ray (Figure 5h), MR (3D UTE: Figure 5e,f) and MS TSE (Figure 5g) images. As expected the lesion sizes in the MS TSE images appear much smaller than in the 3D UTE images.

A hidden caries of category CII is presented in Figure 6. The intraoral picture shows only a conspicuous area before dental treatment (Figure 6a). The lesion shows a bright signal in the 3D UTE (Figure 6d) image ranging into the proximity of the pulp, but this is not visible in the TSE (Figure 6e). In the X-ray image (Figure 6f), an almost negligible lesion with safe distance to the pulp is identified. Excavation revealed a large caries lesion (Figure 6c), which confirms the lesion size apparent in the 3D UTE image.

A CIII secondary caries lesion is shown in Figure 7. Owing to the superimposed filling material along the unresolved dimension, the lesion is not clearly visible in the X-ray image (Figure 7f). However, the lesion can be

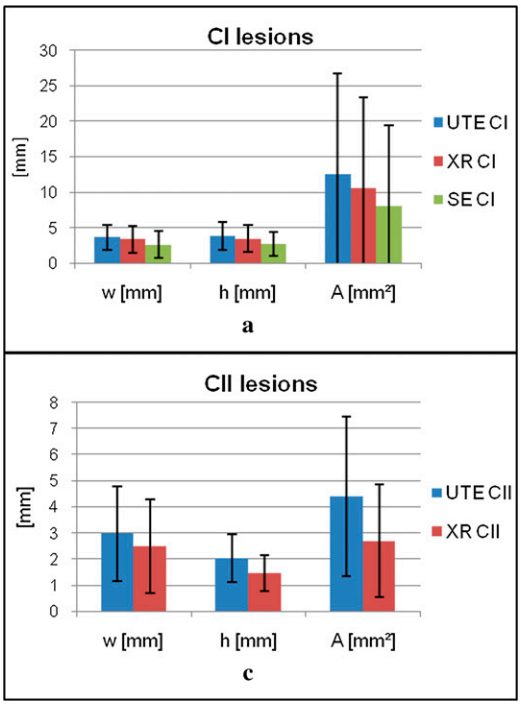

	$P_{SE\text{-}UTE}$	$P_{SE\text{-}XR}$	$P_{UTE\text{-}XR}$
width [mm]	<0.01	<0.01	<0.05
height [mm]	<0.01	<0.01	<0.01
d_{pulp} [mm]	<0.01	0.22	<0.01
area [mm²]	<0.01	<0.01	<0.01

b

	$P_{SE\text{-}UTE}$
width [mm]	<0.01
height [mm]	<0.01
d_{pulp} [mm]	<0.01
area [mm²]	<0.01

d

Figure 3 Two-dimensional lesion extend and area of all three imaging techniques and significance of the differences for lesions of categories CI (a, b) and CII (c, d). CI, class 1; CII, class 2; d_{pulp}, minimal distance between lesion and pulp; SE, spin echo; UTE, ultrashort echo time; XR, X-ray

clearly assessed by 3D UTE (Figure 7d). Again, excavation revealed a large caries lesion (Figure 7c), indicating the correct assessment of the lesion dimensions by 3D UTE.

The qualitative comparison between the X-ray image of the impression and the *in vivo* MR and X-ray images is shown in Figure 8. The lesion shape after excavation was estimated from the radiograph of the impression and transferred to the *in vivo* images. The lesion extensions from the impressions of the *in situ* measurements confirm the lesion size in the 3D UTE images and the respective underestimation of the caries lesions in the X-ray images.

Discussion

This clinical study confirms the applicability of 3D UTE MRI for the identification of caries lesions. The direct comparison to the clinical standard radiograph and to conventional spin-echo imaging reveals at least a similar sensitivity of 3D UTE MRI to X-rays and clearly shows the limitations of conventional spin-echo techniques, especially for the identification of small lesions. Limitations of 3D UTE owing to metal artefacts caused by dental fillings were less severe than expected. In 39 randomly enrolled patients, only 14 teeth could not be sufficiently assessed, although the

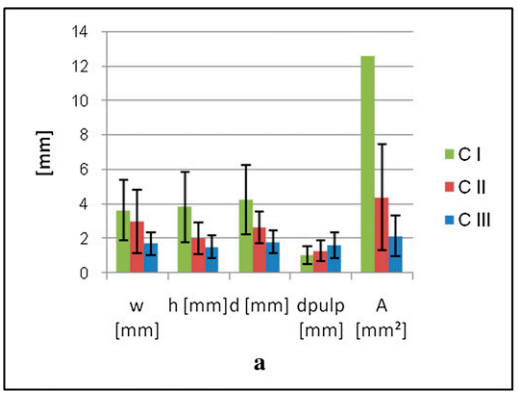

	$P_{CI\text{-}CII}$	$P_{CI\text{-}CIII}$	$P_{CII\text{-}CIII}$
width [mm]	0.1	<0.01	<0.01
height [mm]	<0.01	<0.01	<0.05
depth [mm]	<0.01	<0.01	<0.01
d_{pulp} [mm]	0.09	<0.01	<0.05
area [mm²]	<0.01	<0.01	<0.01

b

Figure 4 (a) Geometrical properties of the lesions in the different categories obtained by the three-dimensional ultrashort echo time (3D UTE) technique. Figure 1b shows the significance of the differences. The standard deviation (±14.2 mm) for the CI area is omitted in the visualization. CI, class 1; CII, class 2; CIII, class 3; d_{pulp}, minimal distance between lesion and pulp.

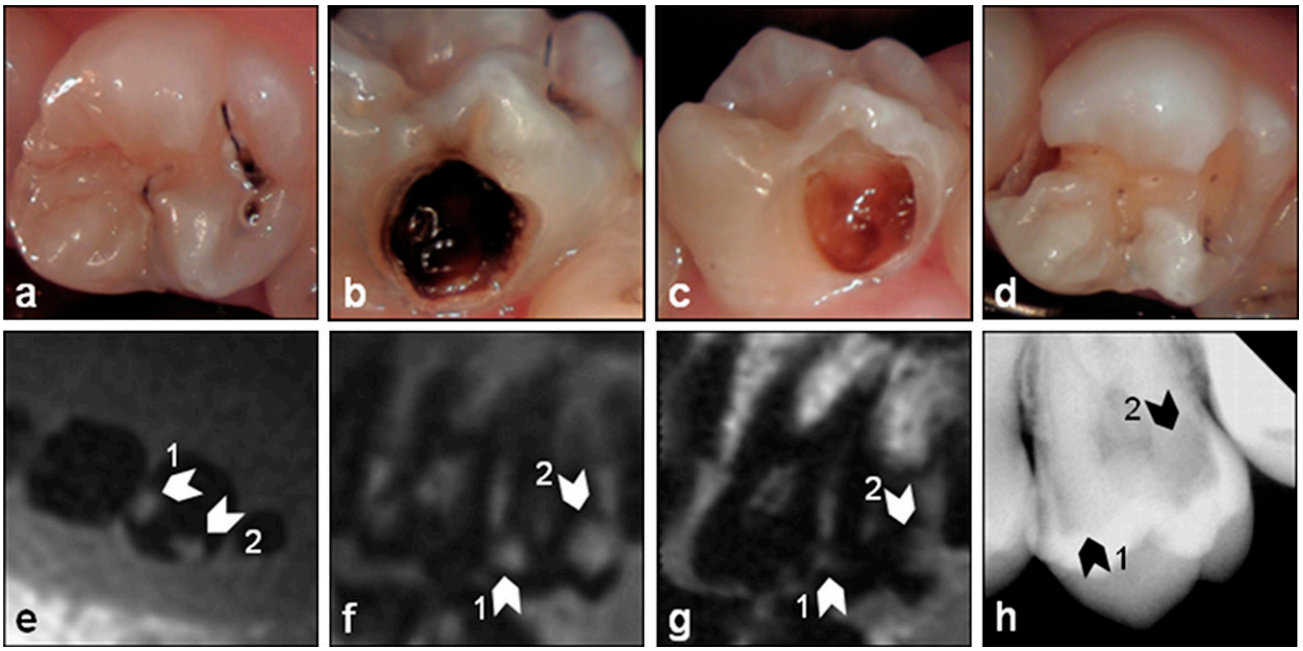

Figure 5 Smooth surface caries (CI): intraoral images (a, occlusal; b, bucal) prior to the dental treatment and the images (c, bucal; d, occlusal) after excavation of the lesions and the respective (e) transversal and (f) parasagittal three-dimensional ultrashort echo time (g) multislice turbo spin-echo and (h) X-ray images of the tooth. The white arrows in the MR images and the black arrows in the X-ray image indicate the lesions

patients presented with gold ($n = 3$), cement ($n = 24$), amalgam ($n = 104$) and composite ($n = 267$) fillings and gold ($n = 70$) and ceramic ($n = 6$) crowns. In total, four lesions visible using X-rays were missed by 3D UTE owing to the superimposed metal artefacts. Interestingly, 24 lesions were identified solely by 3D UTE. This can partly be attributed to the three-dimensional nature of the 3D UTE technique, which appears especially advantageous in cases where the X-ray is limited by structures superimposed along the unresolved dimension. However, the differences in the lesion dimension and the superior visibility of approximal/hidden lesions with 3D UTE are more likely caused by the pathogenesis of caries.

The limited performance of conventional MRI for imaging of mineralized components is caused by the lack of protons and the very short spin–spin relaxation rates due to the susceptibility interfaces in the mineral structures. Formation of a sensible MRI signal from the dentine and enamel layers requires an increase of unbound water and a reduction of the random dephasing of the spins.

The pathogenesis of caries involves local acid accumulation due to the bacterial inflammation, followed by a demineralization and finally breakdown of the mineral structure. In the early stage of lesion formation, the dominant effect results in a local proton density increase due to acid formation and by possible penetration of saliva into the lesions through the increasingly demineralized porous structures in the enamel. At a later stage, the steadily increasing demineralization causes substantial breakdown of the microscopic mineral structures, which results in fluid pools within the surrounding almost intact mineral structures.

The observed signal behaviour in MRI is well supported by the pathogenesis. The initial local increase in acids and saliva results in a local increase of the proton concentration and hence yields a stronger local magnetization. The concomitant initial decay of the local mineralization simultaneously causes a slight decrease of the local random dephasing, and consequently a slight but significant increase of the local T_2^* relaxation time ($T^*_{2\,\text{dentine}} = 324 \pm 94$; $T^*_{2\,\text{lesion}} = 649 \pm 399$ μs).[35] This increase of T_2 and T_2^* in the early stage of carious lesion formation is probably not large enough to be assessed by conventional imaging techniques. With increasing demineralization, however, the local magnetization as well as the T_2^* relaxation time further increases, yielding a sensible MR signal even with conventional spin-echo MR imaging techniques.

Thus the different identified classes likely indicate caries lesions at different stages. Lesions not visible using X-rays but visible by 3D UTE (CIII—lesions) indicate very early lesions/demineralization with no substantial breakdown of the microscopic mineral structure. Since the lesion visibility with X-rays is governed by its mineral content, the slight demineralization does not ensure sufficient contrast in the projective X-ray images. This hypothesis is supported by the significantly smaller extent of CIII lesions than CI/CII lesions, which indicates early stage lesions. With increasing demineralization and respective breakdown of the mineral structure, the lesion size increases (CII/CI) as well as the visibility of the lesion

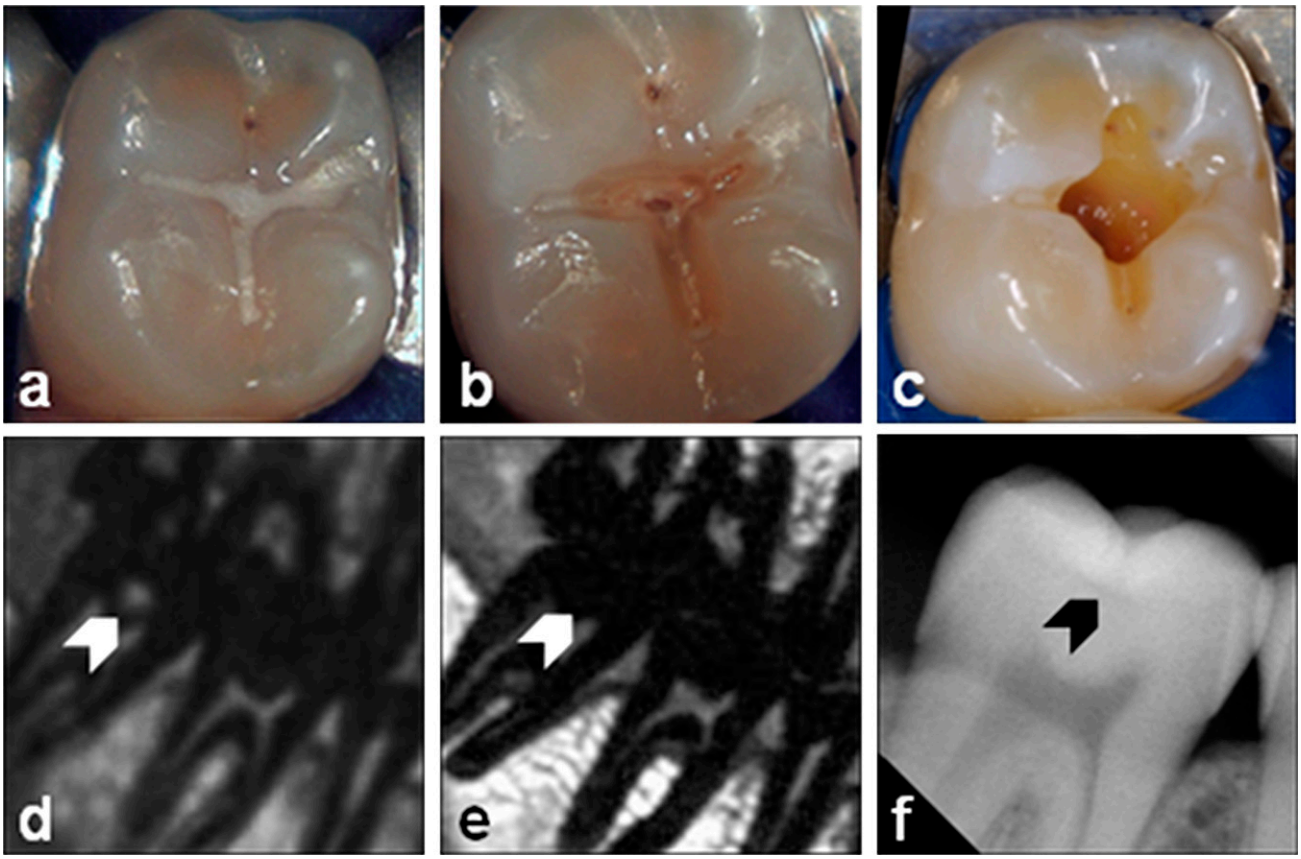

Figure 6 Occlusal (hidden) caries (CII): intraoral pictures of dental treatment (a) prior to the treatment, (b) after fissure sealant removal and (c) after excavation, and the respective three-dimensional ultrashort echo time (d) multislice turbo spin-echo (e) and X-ray (f) images. The white arrows in the MR images and the black arrow in the X-ray image indicate the lesion

with X-ray imaging (CII) and, finally, even in conventional spin-echo MRI (CI).

From clinical routine, it is well known that the lesion extent is often underestimated by X-ray imaging, indicating only a limited performance using X-rays for the identification of the accurate border of the bacterial inflammation and related caries lesion. From the qualitative assessment after excavation, the MRI-derived spatial extent of the lesion appears to match more accurately the diseased area than the respective X-ray-derived values. These results indicate that MRI may be able to provide a more accurate assessment of the real lesion extent and a better estimation of its distance to the pulp.

In direct comparison, the MR images contain more detailed information of the lesion size and especially the distance between the lesion and the pulp than the X-ray images. Since depending on the progress of the lesion and on the extent of dental destruction, different treatment options need to be chosen; the application of MRI may facilitate a more tailored treatment of caries lesions. Especially for early demineralization and initial lesions, the possibility of repeated imaging for therapy monitoring appears to be attractive.[36] Parts of the observed inferior performance of X-ray may be attributed to the averaging done along the unresolved dimension, which might be addressed by tomographic X-ray-based imaging approaches. But even though cone beam computed tomography may provide the required tomographic information because of the related high X-ray dose and strong artefacts caused by metals, its application in caries detection and diagnosis is not indicated.[37–39]

In the previous work published by Tymofiyeva et al,[33] a conventional MS TSE imaging technique with high spatial resolution of $0.3 \times 0.3 \times 0.35\,mm^3$ and a rather long echo time of 12 ms has been applied. For ensuring sufficient image contrast, the oral cavity was partly filled with contrast medium doped agarose gel. In this study, it has been shown that the lesion size in the non-contrast-enhanced MS TSE images (TE = 8.1 ms) underestimates the real lesion size and a signal can likely only be observed in cases where the mineral structure of the tooth is already destroyed. Therefore, the bright signal in the MS TSE scans must most likely be attributed to contrast media leaking into the caries lesion instead of its direct visualization. The high resolution used in the study of Tymofiyeva might not be necessary. In the present study no caries lesion was missed even though a three-fold lower resolution has been used. Tymeofiyeva et al[33] motivated the usage of a spin-echo technique by its high

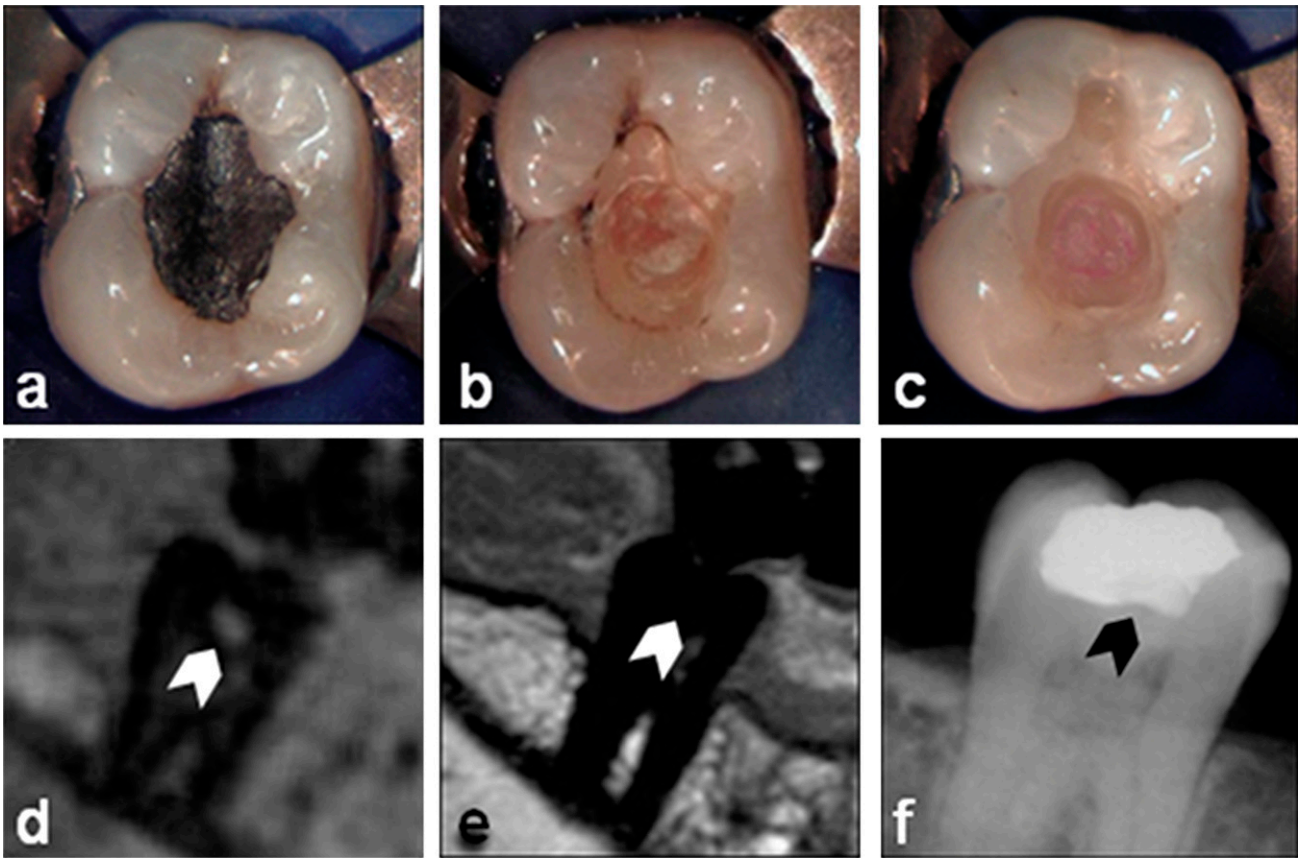

Figure 7 Secondary caries (CIII): intraoral pictures of dental treatment (a) prior to the treatment, (b) after filling removal and (c) after excavation, and the respective three-dimensional ultrashort echo time (d) multislice turbo spin-echo (e) and X-ray (f) images. Lesion position is marked by an arrow

robustness towards artefacts caused by dental fillings and related susceptibility interfaces. Our study shows that the MS TSE and the 3D UTE techniques show a similar artefact level from dental filling materials. None of the 14 teeth that had to be excluded showed superior image quality in MS TSE, as indicated previously.[40]

Although this study proved the potential of 3D UTE for imaging of caries lesions, several obstacles have to be considered before a wide clinical application appears possible. In X-ray images a clear delineation between the different mineral structures of the tooth is possible. In conventional caries, diagnostic lesions are categorized in four classes depending on the extensions of the lesion inside the different structures. According to this classification, different steps of dental treatment have to be chosen. Since these classifications cannot directly be transferred to dental MRI, new classification systems have to be established in future clinical studies. A further major limiting factor is the intrinsically poor SNR of MRI. All data presented in this study have been acquired on a high-field (3 T) whole-body clinical MR system. The related high imaging costs and rather long acquisition times will likely restrict the application of MRI to clinical research. Prior to translation into clinical routine, dedicated dental systems enabling lower imaging costs, easier installation and maintenance and more rapid data acquisition are required. Whether these systems will meet the required SNR constraints remains to be proven. The likely drop in SNR may be addressed by usage of an intraoral coil as published earlier.[41] Further limitations may rise from dental filling materials. In the case of conductive materials, eddy currents may cause local field distortions causing image blur in the 3D UTE technique. Ferromagnetic materials, such as nickel and cobalt, which are used especially in older alloys, dental prostheses, retainers and brackets, may cause severe image degradation. In contrast to the long-ranging banding and streaking artefacts well known from cone beam CT, the nature of artefacts rising in MRI is a local image degradation, which often does not even impact neighbouring teeth. Several correction approaches for MS TSE sequences have already been published, some of them even applicable for gradient echo sequences or non-selective sequences like 3D UTE. Since in the investigated cohort only a small fraction of the investigated teeth could not be analysed, the limitations appear less severe than expected. This may be attributed to the UTE used.[42–47]

In summary, the identification of caries lesions by means of UTE MRI appears feasible. In comparison

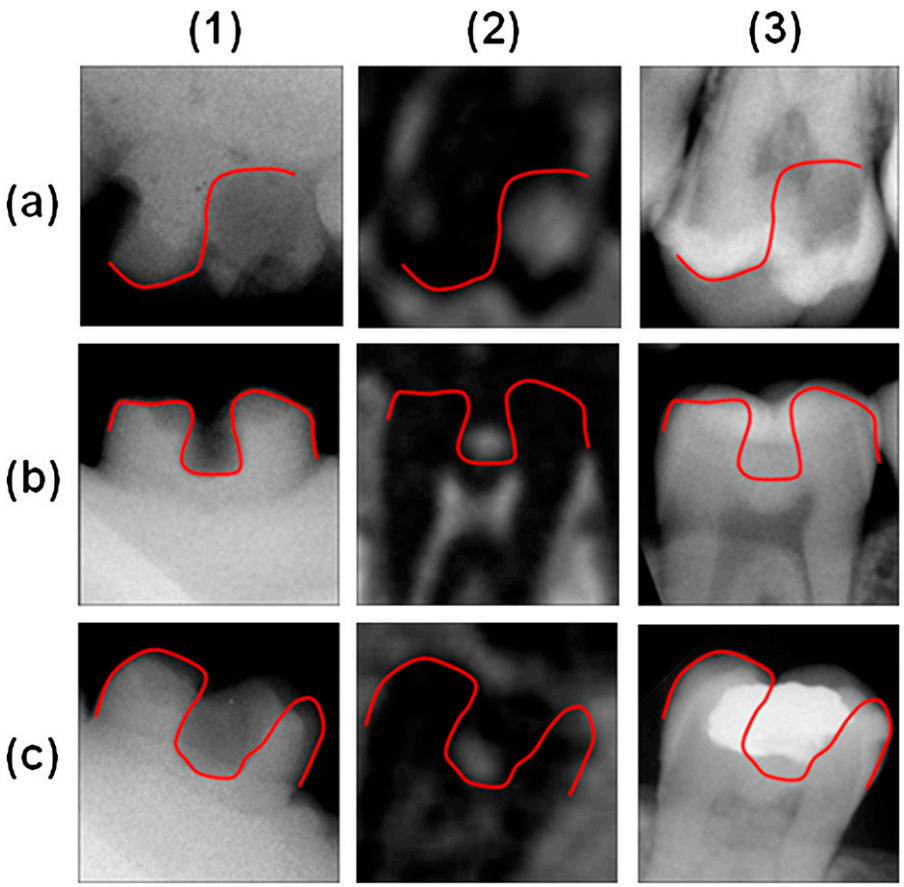

Figure 8 *In situ* measurements: comparison between (1) X-ray of the impression, the appearance of the respective lesion in (2) ultrashort echo time and (3) intraoral X-ray of (a) a smooth surface caries, (b) a hidden caries and (c) a secondary caries lesion

with the clinical standard, 3D UTE MRI has shown a similar sensitivity to intermediated and progressed lesions and clearly outperforms X-ray as well as conventional spin-echo MRI techniques for early stage lesion. Its high sensitivity may enable new applications, such as monitoring of remineralization therapy, and provide a more accurate assessment of the lesion dimension as available from X-ray imaging. Whether its limited spatial resolution, the prolonged acquisition time and the likely higher costs of imaging will avoid wide clinical application of the suggested technique is still unclear.

Funding

The study was funded by Sirona Dental Systems.

Conflict of interest

The funder had no role in any data collection and analysis or preparation of the manuscript but was involved in the study design.

Acknowledgements

VR, BH, AKB, EH and JU conceived and designed the experiments. AKB developed the sequence protocol, performed the data acquisition and drafted the manuscript. VR and AB were involved in the development of the sequence. VR made substantial contributions to conception and design and revised the manuscript critically for important intellectual content. CH recruited the patients. AKB and CH performed the analysis and interpretation of data. BH, AMG and FJ supervised the data analysis and the interpretation of the diagnostic findings.

References

1. Shafiei F, Honda E, Takahashi H, Sasaki T. Artifacts from dental casting alloys in magnetic resonance imaging. *J Dent Res* 2003; **82**: 602–606.
2. van Luijk JA. NMR: dental imaging without X-rays? *Oral Surg Oral Med Oral Pathol* 1981; **52**: 321–324.
3. Christianson R, Lufkin RB, Abemayor E, Hanafee W. MRI of the mandible. *Surg Radiol Anat* 1989; **11**: 163–169.
4. Leslie A, Fyfe E, Guest P, Goddard P, Kabala JE. Staging of squamous cell carcinoma of the oral cavity and oropharynx: a comparison of MRI and CT in T- and N-staging. *J Comput Assist Tomogr* 1999; **23**: 43–49.
5. Manfredini D, Guarda-Nardini L. Agreement between Research Diagnostic Criteria for Temporomandibular Disorders and magnetic resonance diagnoses of temporomandibular disc

displacement in a patient population. *Int J Oral Maxillofac Surg* 2008; **37**: 612–616.
6. Helenius LMJ, Tervahartiala P, Helenius I, Al-Sukhun J, Kivisaari L, Suuronen R, et al. Clinical, radiographic and MRI findings of the temporomandibular joint in patients with different rheumatic diseases. *Int J Oral Maxillofac Surg* 2006; **35**: 983–989.
7. Sener S, Akgänlü F. MRI characteristics of anterior disc displacement with and without reduction. *Dentomaxillofac Radiol* 2004; **33**: 245–252.
8. Chen YJ, Gallo LM, Meier D, Palla S. Dynamic magnetic resonance imaging technique for the study of the temporomandibular joint. *J Orofac Pain* 2000; **14**: 65–73.
9. Tymofiyeva O, Proff P, Richter E-J, Jakob P, Fanghaenel J, Gedrange T, et al. Correlation of MRT imaging with real-time axiography of TMJ clicks. *Ann Anat* 2007; **189**: 356–361.
10. Orhan K, Nishiyama H, Tadashi S, Shumei M, Furukawa S. MR of 2270 TMJs: prevalence of radiographic presence of otomastoiditis in temporomandibular joint disorders. *Eur J Radiol* 2005; **55**: 102–107.
11. Gray CF, Redpath TW, Smith FW, Staff RT. Advanced imaging: Magnetic resonance imaging in implant dentistry. *Clin Oral Implants Res* 2003; **14**: 18–27.
12. Nasel C, Gahleitner A, Breitenseher M, Czerny C, Solar P, Imhof H. Dental MR tomography of the mandible. *J Comput Assist Tomogr* 1998; **22**: 498–502.
13. Aguiar MF, Marques AP, Carvalho ACP, Cavalcanti MG. Accuracy of magnetic resonance imaging compared with computed tomography for implant planning. *Clin Oral Implants Res* 2008; **19**: 362–365.
14. Imamura H, Sato H, Matsuura T, Ishikawa M, Zeze R. A comparative study of computed tomography and magnetic resonance imaging for the detection of mandibular canals and cross-sectional areas in diagnosis prior to dental implant treatment. *Clin Implant Dent Relat Res* 2004; **6**: 75–81.
15. Gray CF, Redpath TW, Smith FW. Magnetic resonance imaging: a useful tool for evaluation of bone prior to implant surgery. *Br Dent J* 1998; **184**: 603–607.
16. Tutton LM, Goddard PR. MRI of the teeth. *Br J Radiol* 2002; **75**: 552–562.
17. Tymofiyeva O, Rottner K, Jakob PM, Richter EJ, Proff P. Three-dimensional localization of impacted teeth using magnetic resonance imaging. *Clin Oral Investig* 2010; **14**: 169–176.
18. Schreiner LJ, Cameron IG, Funduk N, Miljković L, Pintar MM, Kydon DN. Proton NMR spin grouping and exchange in dentin. *Biophys J* 1991; **59**: 629–639.
19. Funduk N, Kydon DW, Schreiner LJ, Peemoeller H, Miljković L, Pintar MM. Composition and relaxation of the proton magnetization of human enamel and its contribution to the tooth NMR image. *Magn Reson Med* 1984; **1**: 66–75.
20. Baumann M, Doll GM, Zick K. Stray-field imaging (STRAFI) of teeth. *Oral Surg Oral Med Oral Pathol* 1993; **75**: 517–522.
21. Appel TR, Baumann MA. Solid-state nuclear magnetic resonance microscopy demonstrating human dental anatomy. *Oral Surg Oral Med Oral Pathol Oral Radiol Endod* 2002; **94**: 256–261.
22. Wu Y, Chesler DA, Glimcher MJ, Garrido L, Wang J, Jiang HJ, et al. Multinuclear solid-state three-dimensional MRI of bone and synthetic calcium phosphates. *Proc Natl Acad Sci U S A* 1999; **96**: 1574–1578.
23. Gruwel MLH, Latta P, Tanasiewicz M, Volotovskyy V, Šramek M, Tomanek B. MR imaging of teeth using a silent single point imaging technique. *Appl Phys A Mater Sci Process* 2007; **88**: 763–767.
24. Idiyatullin D, Corum C, Moeller S, Prasad HS, Garwood M, Nixdorf DR. Dental magnetic resonance imaging: making the invisible visible. *J Endod* 2011; **37**: 745–752.
25. Weiger M, Pruessmann KP, Bracher AK, Köhler S, Lehmann V, Wolfram U, et al. High-resolution ZTE imaging of human teeth. *NMR Biomed* 2012; **25**: 1144–1151.
26. Gatehouse PD, Bydder GM. Magnetic resonance imaging of short T2 components in tissue. *Clin Radiol* 2003; **58**: 1–19.
27. Boujraf S, Hofmann C, Ulrici J, Hell E, Rasche V. Microstructural assessment of dental tissues by quantitative MRI using ultra-short echo times (UTE): initial in vivo evaluation. Proceedings of the ISMRM Seventeenth Annual Meeting; Hawaii, HI, USA; 2009.
28. Cate ART. *Oral histology: development, structure, and function.* 5th edn. St. Louis, MO: Mosby-Year Book; 1998.
29. Bracher AK, Hofmann C, Bornstedt A, Boujraf S, Hell E, Ulrici J, et al. Feasibility of ultra-short echo time (UTE) magnetic resonance imaging for identification of carious lesions. *Magn Reson Med* 2011; **66**: 538–545.
30. Weglarz WP, Tanasiewicz M, Kupka T, Skórka T, Sułek Z, Jasiński A. 3D MR imaging of dental cavities-an in vitro study. *Solid State Nucl Magn Reson* 2004; **25**: 84–87.
31. Lloyd CH, Scrimgeour SN, Chudek JA, Hunter G, MacKay RL. Application of magnetic resonance microimaging to the study of dental caries. *Caries Res* 2000; **34**: 53–58.
32. Lloyd CH, Scrimgeour SN, Chudek JA, Hunter G, MacKay RL. Magnetic resonance microimaging of carious teeth. *Quintessence Int* 1997; **28**: 349–355.
33. Tymofiyeva O, Boldt J, Rottner K, Schmid F, Richter E-J, Jakob PM. High-resolution 3D magnetic resonance imaging and quantification of carious lesions and dental pulp in vivo. *MAGMA* 2009; **22**: 365–374.
34. Whaites E. *Essentials of dental radiography and radiology.* 4th edn. Oxford, UK; Elsevier Health Sciences; 2006.
35. Bracher AK, Bornstedt A, Ulrici J, Hell E, Rasche V. In vivo and in vitro T_2^* quantification of carious lesions by ultra-short echo-time (UTE) MRI. Proceeding of the International Society for Magnetic Resonance in Medicine, Montreal, Canada; 2011.
36. Usha C, Sathyanarayanan R. Dental caries: a complete change-over (Part I). *J Conserv Dent* 2009; **12**: 46–54.
37. European Commission. Radiation protection no. 172: cone beam CT for dental and maxillofacial radiology, Evidence Based Guidelines. Luxembourg: Directorate-General for Energy Directorate D—Nuclear Energy Unit D4—Radiation Protection; 2012.
38. Schulze R, Heil U, Gross D, Bruellmann DD, Dranischnikow E, Schwanecke U, et al. Artefacts in CBCT: a review. *Dentomaxillofac Radiol* 2011; **40**: 265–273.
39. Claus EB, Calvocoressi L, Bondy ML, Schildkraut JM, Wiemals JL, Wrensch M. Dental X-rays and risk of meningioma. *Cancer* 2012; **118**: 4530–4537.
40. Boujraf S, Hofmann C, Maschka R, Ulrici J, Hell E, Haller B, et al. In-vitro quantification of dental filling induced artifacts in dental magnetic resonance imaging using ultrashort echo time (UTE) at 3 Tesla. Proceedings of the International Society for Magnetic Resonance in Medicine; 18–24 April 2009; Honolulu, HI. Honolulu, HI: ISMRM; 2009.
41. Tymofiyeva O, Rottner K, Gareis D, Boldt J, Schmid F, Lopez MA, et al. In vivo MRI-based dental impression using an intraoral RF receiver coil. *Concepts Magn Reson Part B Magn Reson Eng* 2008; **33B**: 244–251.
42. Mount GJ, Hume WR. A new cavity classification. *Aust Dent J* 1998; **43**: 153–159.
43. Mount GJ, Hume WR. A revised classification of carious lesions by site and size. *Quintessence Int* 1997; **28**: 301–303.
44. Lu W, Pauly KB, Gold GE, Pauly JM, Hargreaves BA. SEMAC: slice encoding for metal artifact correction in MRI. *Magn Reson Med* 2009; **62**: 66–76.
45. Koch KM, Lorbiecki JE, Hinks RS, King KF. A multispectral three-dimensional acquisition technique for imaging near metal implants. *Magn Reson Med* 2009; **61**: 381–390.
46. Carl M, Du J, Koch KM. Investigations on Imaging Near Metal with Combined 3D UTE-MAVRIC. Proceedings of the International Society for Magnetic Resonance in Medicine; 7–13 May 2011; Montreal, Canada. Montreal, Canada: ISMRM; 2011.
47. Cox RJ, Kau CH, Rasche V. Three-dimensional ultrashort echo magnetic resonance imaging of orthodontic appliances in the natural dentition. *Am J Orthod Dentofacial Orthop*. 2012; **142**: 552–561.